Harmonic peaks of stripe phases in cuprates

B. Phillabaum and E. W. Carlson
Department of Physics, Purdue University, West Lafayette, Indiana 47907, USA
(Received 17 May 2007; revised manuscript received 31 January 2008; published 25 March 2008)

We calculate the relative intensities of the main incommensurate and third harmonic peaks expected from elastic neutron scattering for various stripe phases observed in nickelates and some cuprate superconductors. We consider vertical and diagonal stripes and compare both site- and bond-centered configurations of the domain walls. Upon comparing the calculated ratio of the main incommensurate peaks to the next harmonic peaks in these configurations to the background and errors in neutron scattering experiments, we conclude that in most cases in the cuprates, the harmonic peaks expected from stripes are too weak to be detected.

DOI: 10.1103/PhysRevB.77.104526 PACS number(s): 74.72.−h, 71.27.+a, 74.25.Ha, 75.40.Cx

I. INTRODUCTION

Strong electronic correlations can lead to a proliferation of competing ground states and possibly new phases. There is evidence that real-space electronic structure is a prominent feature of the phase diagram of many strongly correlated materials.[1] Understanding where and when real-space order happens is crucial to unravelling much of the novel electronic properties of these materials. One candidate set of real-space electronic order, akin to electronic liquid crystals because they break the rotational symmetry of the point group of the host crystal, is commonly referred to as stripes. Evidence linking these structures to superconductivity has been seen in some families of cuprate superconductors,[2–7] although evidence of stripe phases remains elusive in other families of cuprates.

In their fully ordered state, stripes are a unidirectional, interleaved spin and charge density wave, in which charge stripes form antiphase domain walls in an otherwise antiferromagnetic texture. We are concerned here only with the spin degrees of freedom. Elastic magnetic incommensurate (IC) peaks consistent with static spin stripe order have been observed in nickelate compounds, and also in a subset of cuprate superconductors, namely, $La_{2-x}Ba_xCuO_4$, $La_{1.6-x}Nd_{0.4}Sr_xCuO_4$, $La_2CuO_{4+\delta}$, and $La_{2-x}Sr_xCuO_4$.[8] The validity of the stripe interpretation of the magnetic response in the cuprates has been called into question based on the low energy neutron results for three main reasons. First, the observed patterns are usually fourfold symmetric, whereas a single domain of spin stripes should produce a twofold symmetric scattering pattern. Second, while low energy spin wave cones are observed in the nickelates, spin wave cones are not observed in the cuprates. Rather, the incommensurate peaks are observed to disperse inward toward the (π,π) peak. Finally, no satellite peaks (third harmonic peaks) have been observed.

Concerning the first point, the observation of fourfold symmetric IC spin peaks is certainly consistent with a fourfold symmetric pattern such as checkerboard phases. However, when considered along with data on elastic incommensurate *charge* peaks in materials where it is available, simple checkerboards are ruled out,[9] whereas stripe patterns are consistent with the observed spin and charge peaks in materials where both have been detected. The fourfold symmetric pattern is also consistent with static stripe phases, in cases where the stripes have a domain structure. Moreover, twofold symmetric patterns have been reported in detwinned crystals.[10,11]

Secondly, the inability to resolve the spin wave cones in cuprates has recently been shown to be due to weak spin coupling across the charge domain walls.[12,13] While static spin stripes must have spin wave cones due to Goldstone's theorem, the intensity is not necessarily uniform. In fact, it is highly peaked toward the (π,π) direction when the effective exchange coupling is weaker across the domain wall than the full nearest-neighbor exchange away from the domain wall.

This paper aims to address the third objection listed above, namely, that if static stripe order is present in the cuprates, third harmonic peaks should have been observed in elastic neutron scattering experiments. As we show below, the third harmonic peaks are expected to be quite weak, and experiments directly measuring Cu moments in cuprates[3,4,6,7,10,14–34] cannot yet rule out even (unphysically sharp) square-wave stripes.

In this paper, we consider both vertical and diagonal stripe configurations, where the domain walls are allowed to be either site centered or bond centered. We discuss the model and method for calculating the expected elastic peak intensities for neutron scattering in Sec. II. The results of these calculations are presented in Sec. III. Finally, in Sec. IV, we discuss our theoretical results in light of experimental results for neutron scattering, comparing the expected ratio of incommensurate peaks to third harmonic peaks with the current experimental signal-to-noise thresholds for a variety of materials and dopings among the nickelates and cuprates.

II. MODEL

Since we are interested in neutron scattering experiments, which directly detect the spins of electrons in a solid, we are concerned then only with the response of the spin degrees of freedom of stripes. We consider ordered spin stripes, which are arrays of antiphase domain walls in an antiferromagnetic background. By symmetry, each domain wall must have some charge density on it.[35] We will assume that the effects of these charge degrees of freedom on the low energy spin degrees of freedom may be subsumed into effective couplings between spins across each domain wall.

For any given spin stripe pattern, the response of the spins in a neutron scattering experiment is related to the dynamical spin structure factor,

$$S(\mathbf{k},\omega) = \sum_f \sum_{i=x,y,z} |\langle f|S^i(\mathbf{k})|0\rangle|^2 \delta(\omega - \omega_f). \quad (1)$$

In the case of elastic scattering, the elastic part of the structure factor is proportional to the square of the Fourier transform of the static spin density:[36,37]

$$S^{\mathrm{el}}(\mathbf{k},\omega) \propto \sum_{\mathbf{q}} |S^z_{\mathbf{q}}|^2 \delta(\mathbf{k}-\mathbf{q})\delta(\omega), \quad (2)$$

where $S^z_{\mathbf{q}} = 1/N \Sigma_{m,n} e^{ia(mq_x+nq_y)} S_{m,n}$, m and n run over the lattice sites in the x and y directions, respectively, a is the lattice spacing, and the spin density $S_{m,n}$ is taken to be in the z direction.

We consider both vertical and diagonal stripes in cases where the domain walls are site or bond centered. Stripes are deemed "vertical" if the modulation vector is oriented parallel to Cu-O or Ni-O bonds; they are "diagonal" if the modulation vector is rotated 45° from this direction. It is not yet clear from diffraction experiments exactly where the domain walls lie,[38] and so we consider both site-centered and bond-centered domain walls. Site-centered domain walls are centered on Cu or Ni sites, while bond-centered domain walls are centered between Cu/Ni sites, i.e., on the oxygen sites. We also consider a variety of spacings between domain walls.

In the case of bond-centered, vertical stripes, the static spin modulation on each Cu/Ni site for a *square-wave profile* may be written as

$$S^{VB}_{m,n}(p) = S(-1)^m(-1)^n(-1)^{(\bar{n})/hp}, \quad (3)$$

where p is the average domain wall spacing, h is the number of domain walls encompassed within a repeat distance a, and S is the net magnetic moment on each site. The local modulation is antiferromagnetic, with a π phase shift in the static magnetic texture of every p sites, caused by

$$\bar{n} \equiv hn - (hn) \bmod a. \quad (4)$$

The average spacing between domain walls is then $p=a/h$. This reduces to the case of integer p when $h=1$. A schematic of the corresponding spin-density modulation for $p=3$, 4, and 5 is shown in Figs. 3(a)–3(c). For noninteger spacing p, this method constructs arrays of site-centered domain walls or arrays of bond-centered domain walls, without mixing the two. (See Ref. 40 for a treatment mixing site- and bond-centered domain walls.) The noninteger spacing p corresponds to the average spacing between gray lines in Fig. 6. For the case of site-centered, vertical stripes, we introduce a multiplier to enforce zero spin density on the sites along the domain wall,

$$S^{VS}_{m,n}(p) = S^{VB}_{m,n}(p)(\delta_{\bar{n},\overline{n+1}}), \quad (5)$$

where $\delta_{i,j}$ is the Kronecker delta.

Diagonal stripes may be defined in a similar manner (see Figs. 4 and 2). For bond-centered, diagonal stripes, this yields

$$S^{DB}_{m,n}(p) = S(-1)^m(-1)^n(-1)^{[\overline{(m+n)}]/hp}. \quad (6)$$

For the diagonal, site-centered case, a multiplier is introduced to enforce zero spin density on the sites along the domain wall,

$$S^{DS}_{m,n}(p) = S^{DB}_{m,n}(p)(\delta_{\overline{n+m},\overline{m+n+1}}). \quad (7)$$

There are two main effects of doping on the stripe structure. As doping x (i.e., the planar hole concentration) is increased, the spacing p between domain walls can go down. The second effect is that the linear density of holes along the domain wall can increase with doping. For a given doping and spacing between domain walls, the linear hole density is

$$\rho = xp(x). \quad (8)$$

This charge density is spread out in some envelope transverse to the domain wall.

In the site-centered case, the spin density is constrained by symmetry to be zero on the atomic sites which lie on the domain wall, and so the minimum width for the domain wall, and therefore the minimum extent of the envelope of the doped holes transverse to the domain walls, is one lattice site. Of course in real materials, charge will leak out beyond this and diminish the static magnetic moment on sites which *neighbor* the domain wall as well. It will suffice for our purposes to consider the thinnest domain wall possible that in which all of the doped charge density is on the sites on the domain wall. This is the limit of "square-wave" site-centered stripes. Although artificially sharp, these configurations provide an upper bound on the allowed intensity of the third harmonic peaks. Any smoother profile of the charge and spin density will diminish the third harmonic peaks further. For bond-centered stripes, a similar square-wave limit is even more unphysical, since it does not take into account the reduction of the spin density as holes are doped into the domain walls. In this paper, we focus on square-wave profiles as a limiting case. As we will see, with current signal-to-noise ratios in the cuprates, experiments directly measuring Cu moments cannot yet rule out the possibility of third harmonic peaks from even unphysically sharp square-wave stripes if they are site centered.

III. RESULTS

A. Site-centered square-wave limit

We first present results for site-centered stripes using square-wave profiles. Figures 1(a) and 1(c) show the real-space structure of vertical, site-centered stripes of spacings $p=4$ and $p=5$, respectively. In these diagrams, black is used to represent the down spin, white is used to represent the up spin, and gray denotes a static spin moment which is reduced from the full value. In the case of site-centered stripes, sites along the domain walls are constrained by symmetry to have zero static spin moment. Figures 1(b) and 1(d) show the expected elastic neutron scattering response for these configurations. The intensity of each peak is normalized to that of the main incommensurate peaks. Notice that even in this most extreme case of a square-wave profile, the third har-

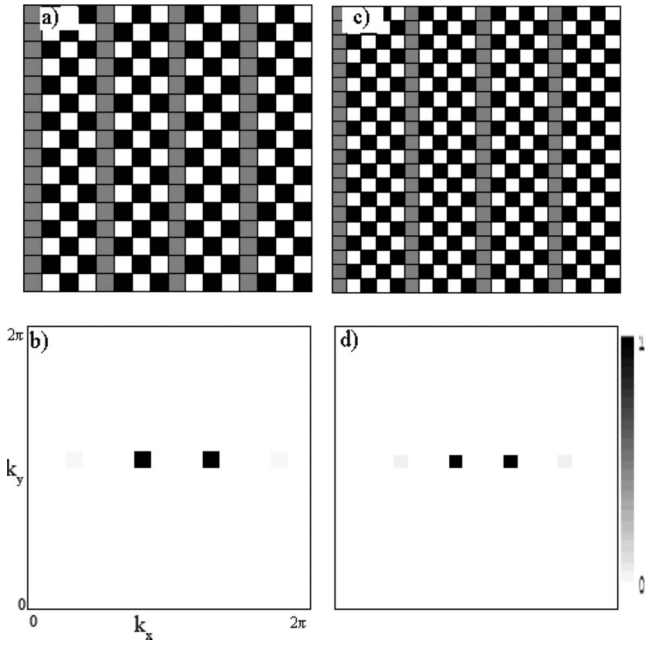

FIG. 1. Vertical, site-centered stripes of spacings $p=4$ and 5 with square-wave profiles. Panels (a) and (c) show the real-space pattern of the spin structure for spacings $p=4$ and $p=5$, respectively. Panels (b) and (d) show the corresponding neutron diffraction patterns, with intensities normalized to that of the main IC peaks. For a spacing $p=4$, the third harmonic peak intensity is $1/34=2.9\%$ of the main IC peaks (Refs. 12 and 45); for $p=5$, it is $1/18=5.5\%$ of the main IC peaks.

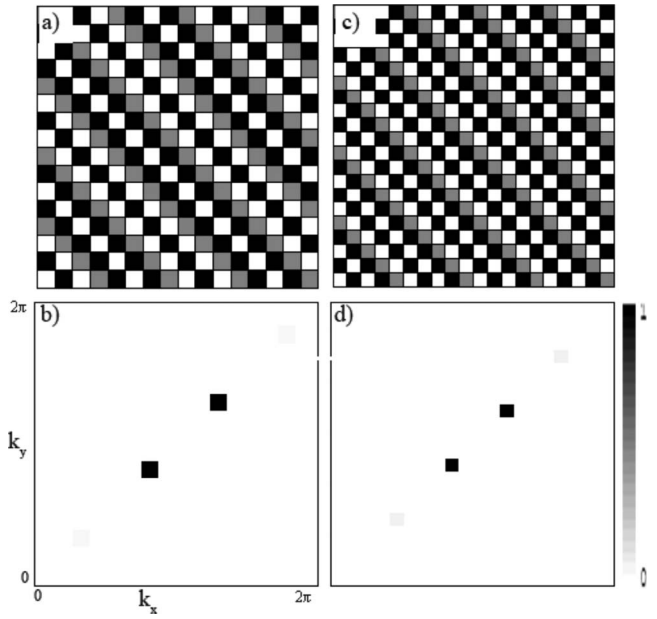

FIG. 2. Diagonal, site-centered stripes of spacings $p=4$ and 5 with square-wave profiles. Panels (a) and (c) show the real-space pattern of the spin structure for spacings $p=4$ and $p=5$, respectively. Panels (b) and (d) show the corresponding neutron diffraction patterns, with intensities normalized to that of the main IC peaks. Intensity ratios are identical to those of Fig. 1.

monic peaks are quite weak. We have not shown the case $p=3$, since for site-centered stripes of odd spacing, peaks at $(0,\pi)$ are extinguished due to symmetry,[12] i.e., the ratio of intensities between the third harmonic and main IC peaks in this case is ∞. For stripes of spacing $p=4$, as happens near the 1/8 anomaly, although the third harmonic peaks are nonzero, they are 34 times weaker than the main IC peaks, as has been noted previously in Refs. 12 and 45. As the spacing p increases, the third harmonic peaks become more pronounced, but they are still 18 times weaker than the main IC peaks at $p=5$. In Sec. IV, we discuss whether third harmonic peaks should be expected to be observed with current experimental capabilities, keeping in mind that in real materials, the domain walls are surely broader due to quantum effects, suppressing the third harmonic peaks even further. The case of diagonal site-centered stripes with square-wave profiles is shown in Fig. 2. The expected ratios for IC to harmonic peaks are the same in this case as for the vertical case. These results are summarized in Table I.

B. Bond-centered square-wave limit

In Figs. 3 and 4, we present results for bond-centered stripes using square-wave profiles. Figures 3(a), 3(c), and 3(e) show the real-space structure of vertical, bond-centered stripes of spacings $p=3$, 4, and 5, respectively. Note that in the bond-centered case, the domain walls lie between sites, and so for a square-wave profile, all sites have the full spin value. This neglects the linear hole density which must reside on each domain wall, reducing the average spin moment per site, as discussed in Sec. II. Figures 3(b), 3(d), and 3(f) show the expected elastic neutron scattering response for the square-wave configurations. When the spacing p between domain walls is odd, bond-centered stripes display third harmonic peaks of finite intensity at $(0,\pi)$; such peaks are forbidden in the site-centered case for odd spacing p.[12] The intensity of the third harmonic peak in the bond-centered case for spacings $p=3$, 4, and 5 with square-wave profiles is suppressed from the value of the main IC peaks by a factor of 4.2, 5.8, and 6.9, respectively. The case of diagonal bond-centered stripes with square-wave profiles is shown in Fig. 4. The expected ratios for third harmonic to IC peaks are the

TABLE I. *Commensurate spacing*: ratio of the main IC peak intensity to the third harmonic peak for square-wave stripes of spacings $p=3$, 4, and 5 for both site-centered and bond-centered configurations of the domain walls. For square-wave profiles, the peak ratios are independent of whether the domain walls are vertical or diagonal.

Domain wall	Spacing	Peak ratio
Site centered	3	∞
Site centered	4	34
Site centered	5	18
Bond centered	3	4.2
Bond centered	4	5.8
Bond centered	5	6.9

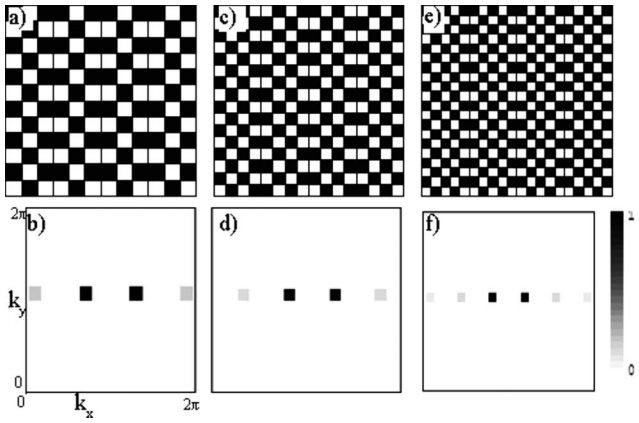

FIG. 3. Vertical, bond-centered stripes of spacings $p=3$, 4, and 5 with square-wave profiles. Panels (a), (c), and (e) show the real-space pattern of the spin structure for spacings $p=3$, $p=4$, and $p=5$, respectively. Panels (b), (d), and (f) show the corresponding neutron diffraction patterns, with intensities normalized to that of the main IC peaks. For a spacing $p=3$, the harmonic peak intensity is $1/4.2=24\%$ of the main IC peaks; for $p=4$, it is $1/5.8=17\%$, and for $p=5$, the third harmonic peak is $1/6.9=14\%$ of the main IC peaks. Note that there is a fifth harmonic peak for $p=5$, which was forbidden in the site-centered case at this spacing.

same in this case as for the vertical case. These results are summarized in Table I.

C. Other cases

In this section, we consider the effects of noninteger spacing p, as well as deviations from the square-wave limit. Using the method outlined in Sec. II, we have studied arrays of domain walls with average spacings from $p=4-\frac{1}{3}$ to $p=4+\frac{1}{3}$. In Table II, we report the ratio of the main IC peak intensity to the third harmonic peak for higher commensurability spacings, i.e., for noninteger, rational p. Real-space figures of these configurations, as well as the expected neutron diffraction pattern, are shown in Figs. 5 and 6. We have focused on spacings near $p=4$, since spacings near this value are most common in underdoped superconducting cuprates which also display IC peaks in neutron scattering. It is important to note that these are the ratios of the largest peak (i.e., the main IC peak) divided by the third harmonic peak. In the bond-centered case, the next largest peak after the main IC peak is the third harmonic peak. The peak ratios of the main IC peaks to the third harmonic peaks are somewhat

TABLE II. *Incommensurate spacing*: ratio of the main IC peak intensity to the third harmonic peak for incommensurate spacings $p=4-\frac{1}{3}$ to $p=4+\frac{1}{3}$ for both site-centered and bond-centered configurations of the vertical and diagonal domain walls.

Incommensurate spacing Domain wall	Spacing	Peak ratio
Site centered	$4-\frac{1}{3}$	89
Site centered	$4-\frac{1}{5}$	70
Site centered	$4-\frac{1}{9}$	61
Site centered	$4+\frac{1}{9}$	45
Site centered	$4+\frac{1}{5}$	41
Site centered	$4+\frac{1}{3}$	35
Bond centered	$4-\frac{1}{3}$	8.5
Bond centered	$4-\frac{1}{5}$	8.8
Bond centered	$4-\frac{1}{9}$	8.95
Bond centered	$4+\frac{1}{9}$	9.0
Bond centered	$4+\frac{1}{5}$	8.9
Bond centered	$4+\frac{1}{3}$	8.7

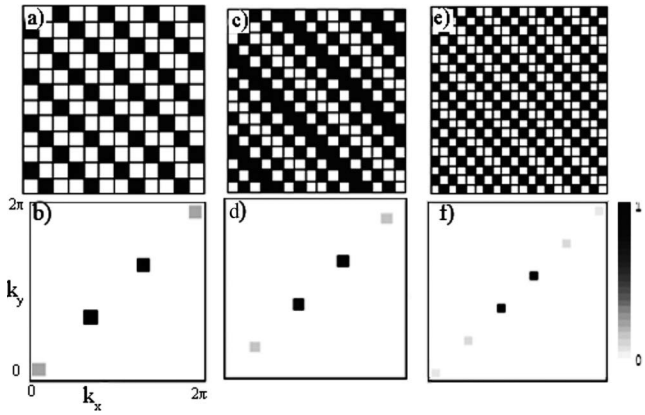

FIG. 4. Diagonal, bond-centered stripes of spacings $p=3$, 4, and 5 with square-wave profiles. Panels (a), (c), and (e) show the real-space pattern of the spin structure for spacings $p=3$, $p=4$, and $p=5$, respectively. Panels (b), (d), and (f) show the corresponding neutron diffraction patterns, with intensities normalized to that of the main IC peaks. Intensity ratios are identical to those of Fig. 3.

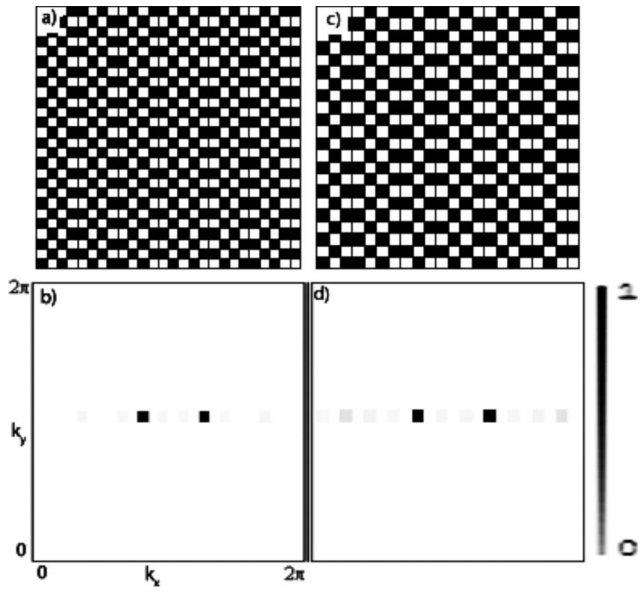

FIG. 5. Higher commensurate bond-centered stripes of spacings $p=4+\frac{1}{3}$ and $p=4-\frac{1}{3}$ with square-wave profiles. Panels (a) and (c) show the real-space pattern of the spin structure for spacings $p=4+\frac{1}{3}$ and $p=4-\frac{1}{3}$, respectively. Panels (b) and (d) show the corresponding neutron diffraction patterns, with intensities normalized to that of the main IC peaks.

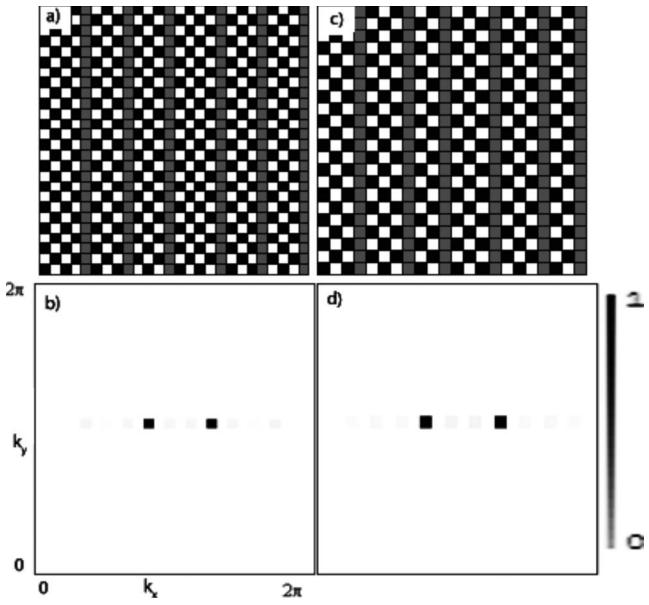

FIG. 6. Higher commensurate site-centered stripes of spacings $p=4+\frac{1}{3}$ and $p=4-\frac{1}{3}$ with square-wave profiles. Panels (a) and (c) show the real-space pattern of the spin structure for spacings $p=4+\frac{1}{3}$ and $p=4-\frac{1}{3}$, respectively. Panels (b) and (d) show the corresponding neutron diffraction patterns, with intensities normalized to that of the main IC peaks.

larger in the higher commensurate case (noninteger, rational p) as compared to the case of integer p. This means that higher commensurabilities make the third harmonic peaks harder to detect, although (in the limit of square-wave profiles) not much harder to detect.

We now briefly consider deviations from the limiting case of square waves we have considered thus far. In the opposite limit of a sinusoidal modulation (whether bond or site centered), the peak ratios become infinite, despite the effects of an underlying lattice, even for arbitrarily high commensurabilities. Because of this, deviations from the square-wave limit we have focused on, toward the sinusoidal limit, rapidly tend toward vanishing third (and higher) harmonic peaks. For example, in the case of vertical, site-centered stripes of spacing $p=4$, a linear interpolation that is 50% of the way between the real-space spin density for the square-wave case and that of the sine wave case has a peak ratio intensity of 120, roughly a threefold increase over the square-wave limit. For an interpolation that is 90% of the way toward the sinusoidal limit, the ratio exceeds 1000. This suggests that even if experiments achieve significantly better resolution, setting experimental constraints on the actual shape of the spin-density wave will likely remain elusive.

IV. DISCUSSION

We now address the central question of this paper: If we interpret incommensurate peaks in neutron scattering experiments on cuprates as arising from stripe structures (see Ref. 38 for a recent review of the relevant data), is this consistent with the lack of observation of magnetic third harmonic peaks given the current experimental facts. Our conclusion is that experiments which directly detect Cu moments cannot yet rule out the presence of third harmonic peaks in cuprates even for the unphysically sharp case of square-wave stripes.

Tables III and IV compare current experimental limits with the expected ratio of the intensity of the main IC peak to that of the next harmonic peak in cuprates. Table V shows corresponding data for the nickelates, for comparison. For each material at a particular chemical doping, we use the incommensurability at the lowest reported energy to determine the nearest stripe spacing which is commensurate with the atomic lattice. From this, we have calculated the expected ratio of the third harmonic peak to the main incommensurate peak for static spin stripes, labeled "peak ratio" in the tables. We use the nearest commensurate spacing, since this enhances the expected intensity from third harmonic peaks. For incommensurate stripe spacings, the intensity from third harmonic peaks is lessened, and the peak ratio will be even higher than what is listed in the table. The ratios P/E and P/B are gleaned from the literature in each case. The ratio of the peak intensity (the height of the peak) to the reported error bars for the measurement is denoted by P/E. The ratio P/B is obtained by dividing the maximum intensity of the IC peaks by the intensity of the background noise in the vicinity of the peaks. Both of these numbers should be compared to the expected peak ratio, i.e., the expected intensity ratio between the main IC peaks and the third harmonic peaks for the limiting cases considered here. The range reported for the calculated peak ratio spans from bond-centered square-wave stripes (the smaller number) to site-centered square-wave stripes (the larger number). It should be emphasized of course that both of these calculated cases have sharper domain walls than should be expected in real materials, where quantum effects serve to broaden the width of the charge domain walls, further suppressing the expected intensity of the third harmonic peaks.

For dopings $x>0.13$, the neutron scattering response in $La_{2-x}Sr_xCuO_4$ (LSCO) develops a measurable gap. In these cases, the stripes are at best quantum disordered, rather than the static, ordered cases considered here. However, it has been recently shown[13] that *even on the quantum disordered side* of the quantum critical point (QCP) between static spin stripes and quantum disordered stripes, the distribution of the energies and intensities of the magnetic response strongly resembles the semiclassical approximation applicable to ordered spin stripes. This strong resemblance has been attributed to the small value of the critical exponent $\eta=0.037 \ll 1$ at the QCP.[13] For dopings $x>0.13$, we compare to the measured incommensurability at the lowest energy for which the signal is discernible. As long as the lowest energies at which there is a response are not too high, the expected intensity ratios at these energies are largely controlled by the corresponding intensity ratios for the static peaks of ordered spin stripes, which is what we have calculated.

$YBa_2Cu_3O_{7-x}$ (YBCO) always has a spin gap, consistent with the spin component of the stripes being quantum disordered. Recent high energy neutron scattering experiments on static stripe-ordered $La_{2-x}Ba_xCuO_4$ (LBCO) and YBCO have demonstrated a universality of the magnetic excitations among LSCO,[29] LBCO,[3,49] and YBCO.[4,50] (see, e.g., Fig. 8.3 in Ref. 38) This universality among the energy spectrum and

TABLE III. Comparison between published experimental sensitivities and the theoretical relative intensity of the main IC peaks to the third harmonic peaks for lanthanum cuprates. The doping in this table is the chemical doping x in La_2CuO_{4+x}, $La_{2-x}Ba_xCuO_4$, $La_{1.875}Ba_{0.125-x}Sr_xCuO_4$, $La_{1.6-x}Nd_{0.4}Sr_xCuO_4$, and $La_{2-x}Sr_xCuO_4$. The ratios P/E and P/B are the ratio of the peak intensity to reported error bars and to the background, respectively, as taken from experiment. A dash in the P/B column indicates that the background was subtracted in published data. The theoretical range of peak ratio encompasses both bond-centered and site-centered square-wave profiles. Spacing denotes the closest commensurate spacing corresponding to the observed IC peaks. Asterisks next to references indicate inelastic neutron scattering; all others are elastic scattering.

Material	Doping	Spacing	P/E	P/B	Peak ratio	Ref.
LCO	0.11	4	10	2–3	5.8–34	31
LCO	0.12	4	7	2–3	5.8–34	32
LBCO	0.125	4	7–9	4	5.8–34	15*, 3*
LBSCO	0.05	4	7	2–3	5.8–34	30
LNSCO	0.15	4	25–30	2	5.8–34	39
LNSCO	0.12	4	7–12	4–20	5.8–34	55 and 41
LSCO	0.014	25	9	—	8.9–9.2	28
LSCO	0.05	10–11	8–9	2–3	8.4–10	10 and 14
LSCO	0.06	10	7	2–3	8.4–10	2*
LSCO	0.10	5	9	2	6.9–18	26*
LSCO	0.12	4	6–9	2	5.8–34	33, 34, and 2*
LSCO	0.14	4	6	2	5.8–34	19*
LSCO	0.15	4	5–6	2–3	5.8–34	27*, 17*
LSCO	0.16	4	7–8	—	5.8–34	29*
LSCO	0.17	4	6	2	5.8–34	25*
LSCO	0.18	4	6	1.7	5.8–34	22*
LSCO	0.20	4	4	2	5.8–34	18*, 20*
LSCO	0.25	4	6–17	2–3	5.8–34	7*, 2*

intensities of magnetic excitations both for spin stripe-ordered and quantum disordered materials is another corroboration that in these materials, the QCP is weak enough, and also that the quantum disordered materials are close enough to the QCP, which the dispersions and intensities at the lowest observable frequencies can still be inferred from the static, spin-ordered patterns as calculated here.[13]

We use two measures from the literature to gauge whether third harmonic peaks are detectable: the ratio of the intensity of the main IC peak to the error bars (P/E) and to the background signal (P/B). Ideally, both of these should be larger than the calculated peak ratio for third harmonic peaks to be

TABLE IV. Comparison between published experimental sensitivities and the theoretical relative intensity of the main IC peaks to the third harmonic peaks for yttrium-based cuprates. The doping in this table is the chemical doping δ in $YBa_2Cu_3O_{6+\delta}$. The ratios P/E and P/B are the ratio of the peak intensity to reported error bars and to the background, respectively, as taken from experiment. A dash in the P/B column indicates that the background was subtracted in published data. The theoretical range of peak ratio encompasses both bond-centered and site-centered square-wave profiles. Spacing denotes the closest commensurate spacing corresponding to the observed IC peaks. Asterisks next to references indicate inelastic neutron scattering.

Material	Doping	Spacing	P/E	P/B	Peak ratio	Ref.
YBCO	0.45	8	6	2	8.1–11	42*
YBCO	0.5	5	3	1.3–2	6.9–18	23*
YBCO	0.6	5	4–12	1.6–2	6.9–18	16*, 4*, 21*, 42*
YBCO	0.7	5	6–9	1.3	6.9–18	43*, 42*
YBCO	0.8	5	14	—	6.9–18	42*
YBCO	0.85	5	7	—	6.9–18	44*
YBCO	0.95	5	5	1.4	6.9–18	42*

TABLE V. Comparison between the experimental signal-to-noise ratio and the expected relative intensity of the main IC peaks to the third harmonic peaks for various materials. The doping in this table is the chemical doping x in La_2NiO_{4+x} and $La_{2-x}Sr_xNiO_4$. The ratios P/E and P/B are the ratio of the peak intensity to reported error bars and to the background, respectively, as taken from experiment. The theoretical range of peak ratio encompasses both bond-centered and site-centered square-wave profiles. Spacing denotes the closest commensurate spacing corresponding to the observed IC peaks. Asterisks next to references indicate inelastic neutron scattering; all others are elastic scattering.

Material	Doping	Spacing	P/E	P/B	Peak ratio	Ref.
LNO	0.13	4	23	500	5.8–34	40
LSNO	0.2	4	13–20	6–7	5.8–34	46 and 47
LSNO	0.225	4	10	25	5.8–34	48
LSNO	0.275	4	8	25–50	5.8–34	51 and 53*
LSNO	0.33	3	12–15	50–100	4–∞	54*
LSNO	0.37	3	11	>80	4–∞	52

detectable. In practice, detection is possible if one of these ratios is sufficiently larger than the expected peak ratio.

In Tables III–V the most likely candidate for third harmonic peak detection is La_2NiO_{4+x} (see Table V), with a peak to background ratio of $P/B \approx 500$, as compared with the theoretical upper limit for the peak ratio, 5.8–34. Indeed, third (and higher) harmonic peaks have been detected in this material.[40] Other good candidates are $La_{2-x}Sr_xNiO_4$ at dopings $x=0.275$ and 0.33.[51,53,54] Contrast the ratios of P/E and P/B in the nickelates with those of the cuprates. Whereas many of the nickelate compounds have peak to background ratios on the order of $P/B \approx 50-100$, exceeding the calculated peak ratio for detection of third harmonic peaks, in the cuprates, this number is typically $P/B \approx 2-3$, far below what is needed to detect third harmonic peaks.

A notable exception is $La_{1.6-x}Nd_{0.4}Sr_xCuO_4$. In this compound, the Nd moments order at low temperature ($T \lesssim 3-8$ K), enhancing the signal, so that $P/B \approx 20$ in Ref. 55. Very recent experiments on this compound have achieved $P/B \approx 2000$, without a clear observation of the third harmonic peak.[57] If it can be established that the Nd moments are indeed reflective of the in-plane Cu ordering, this will place serious constraints on the profile of the spin-density wave. In the undoped case, Nd moments couple to only one copper site (directly through the Cu-O-Nd bond), and coupling to the four adjacent Cu sites in the next plane cancels by symmetry. In this case, it is clear that each Nd moment is "slaving" to one and only one Cu site. However, in the doped case in the low temperature tetragonal phase, Nd moments which are adjacent to a charge stripe have a symmetry-allowed coupling to Cu moments in both adjacent planes, which may affect the intensity of the harmonic peaks. We base our conclusions here on data derived purely from Cu moments.

Even in the presence of a sizable background signal, if the uncertainty in the intensity is small enough, one might hope to be able to detect weak peaks by some signal processing such as fitting the form of the peak. In the cuprates (see Tables III and IV), the ratio of the peak intensity to error is typically $P/E \approx 6-10$. (Again, $La_{1.6-x}Nd_{0.4}Sr_xCuO_4$ (LNSCO) is the anomaly as explained above.) This is on the verge of detection for square-wave bond-centered stripes. Of course, as emphasized before, bond-centered stripes in a real material must have a finite width to the domain wall in order to account for doping, which further diminishes the strength of the third harmonic peaks. Moreover, the ratio P/E is too low to be able to rule out the presence of third harmonic peaks due to square-wave site-centered stripes.

V. CONCLUSIONS

In conclusion, we have calculated the expected intensities for both the main incommensurate peaks and the third harmonic peaks for static spin stripes of various spacings and dopings. Even in limiting cases with overly sharp domain walls which enhance the third harmonic peaks, such as bond-centered and site-centered stripes with square-wave profiles, the third harmonic peaks expected from static spin stripe structures are greatly suppressed as compared to the strength of the main incommensurate peaks. Including effects of higher commensurabilities further diminishes the third harmonic peaks, although not much. On the other hand, relaxing the square-wave limit and tending toward a more sinusoidal modulation rapidly suppresses the strength of the third harmonic. By comparing the intensity of the main IC peak to both the experimental uncertainty and background, we conclude that in the cuprates, none of the experiments which directly measure Cu moments are yet sensitive enough to rule out even the unphysically sharp case of square-wave site-centered stripes.

ACKNOWLEDGMENTS

It is a pleasure to thank Y. Loh, J. Tranquada, D. Yao, and especially A. Boothroyd for helpful discussions. This work was supported in part by the Purdue Research Foundation (E.W.C.), Research Corporation (E.W.C.), and NSF Grant No. PHY-05522918 (B.P.).

[1] E. Dagotto, Science **309**, 257 (2005).
[2] K. Yamada, C. H. Lee, K. Kurahashi, J. Wada, S. Wakimoto, S. Ueki, H. Kimura, Y. Endoh, S. Hosoya, G. Shirane, R. J. Birgeneau, M. Greven, M. A. Kastner, and Y. J. Kim, Phys. Rev. B **57**, 6165 (1998).
[3] J. M. Tranquada, H. Woo, T. G. Perring, G. D. Gu, G. Xu, M. Fujita, and K. Yamada, Nature (London) **429**, 534 (2004).
[4] S. M. Hayden, H. A. Mook, P. D. Dai, T. G. Perring, and F. Dogan, Nature (London) **429**, 531 (2004).
[5] E. W. Carlson, V. J. Emery, S. A. Kivelson, and D. Orgad, in *Concepts in High Temperature Superconductivity*, edited by J. Ketterson and K. Benneman, The Physics of Superconductors Vol. 2 (Springer-Verlag, Berlin, 2004).
[6] S. A. Kivelson, I. P. Bindloss, E. Fradkin, V. Oganesyan, J. M. Tranquada, A. Kapitulnik, and C. Howald, Rev. Mod. Phys. **75**, 1201 (2003).
[7] S. Wakimoto, H. Zhang, K. Yamada, I. Swainson, H. Kim, and R. J. Birgeneau, Phys. Rev. Lett. **92**, 217004 (2004).
[8] See Refs. 5, 6, 38, and 56 for reviews of the relevant data.
[9] The data have not yet ruled out more complicated checkerboard patterns, although these bring about other difficulties as discussed in Ref. 38.
[10] S. Wakimoto, R. J. Birgeneau, M. A. Kastner, Y. S. Lee, R. Erwin, P. M. Gehring, S. H. Lee, M. Fujita, K. Yamada, Y. Endoh, K. Hirota, and G. Shirane, Phys. Rev. B **61**, 3699 (2000).
[11] H. A. Mook, P. Dai, F. Dogan, and R. D. Hunt, Nature (London) **404**, 729 (2000).
[12] D. X. Yao, E. W. Carlson, and D. K. Campbell, Phys. Rev. B **73**, 224525 (2006).
[13] D. X. Yao, E. W. Carlson, and D. K. Campbell, Phys. Rev. Lett. **97**, 017003 (2006).
[14] M. Fujita, K. Yamada, H. Hiraka, P. M. Gehring, S. H. Lee, S. Wakimoto, and G. Shirane, Phys. Rev. B **65**, 064505 (2002).
[15] M. Fujita, H. Goka, K. Yamada, J. M. Tranquada, and L. P. Reghault, Phys. Rev. B **70**, 104517 (2004).
[16] V. Hinkov, S. Pailhes, P. Bourges, Y. Sidis, A. Ivanov, A. Kulakov, C. T. Lin, D. P. Chen, C. Bernhard, and B. Keimer, Nature (London) **430**, 650 (2004).
[17] M. Kofu, H. Kimura, and K. Hirota, Phys. Rev. B **72**, 064502 (2005).
[18] C. H. Lee, K. Yamada, H. Hiraka, C. R. Venkateswara Rao, and Y. Endoh, Phys. Rev. B **67**, 134521 (2003).
[19] T. E. Mason, A. Schroder, G. Aeppli, H. A. Mook, and S. M. Hayden, Phys. Rev. Lett. **77**, 1604 (1996).
[20] S. Wakimoto, R. J. Birgeneau, A. Kagedan, H. Kim, I. Swainson, K. Yamada, and H. Zhang, Phys. Rev. B **72**, 064521 (2005).
[21] H. A. Mook, P. Dai, S. M. Hayden, G. Aeppli, T. G. Perring, and F. Dogan, Nature (London) **395**, 580 (1998).
[22] J. M. Tranquada, C. H. Lee, K. Yamada, Y. S. Lee, L. P. Regnault, and H. M. Ronnow, Phys. Rev. B **69**, 174507 (2004).
[23] C. Stock, W. J. L. Buyers, R. Liang, D. Peets, Z. Tun, D. Bonn, W. N. Hardy, and R. J. Birgeneau, Phys. Rev. B **69**, 014502 (2004).
[24] M. Matsuda, M. Fujita, and K. Yamada, Phys. Rev. B **73**, 140503(R) (2006).
[25] R. Gilardi, A. Hiess, N. Momono, M. Oda, M. Ido, and J. Mesot, Europhys. Lett. **66**, 840 (2004).
[26] R. Gilardi, S. Streule, A. Hiess, H. M. Ronnow, M. Oda, N. Momono, M. Ido, and J. Mesot, Physica B **350**, 72 (2004).
[27] H. Kimura, Physica C **392-396**, 34 (2003).
[28] M. Matsuda, M. Fujita, K. Yamada, R. J. Birgeneau, Y. Endoh, and G. Shirane, Phys. Rev. B **66**, 174508 (2002).
[29] N. B. Christensen, D. F. McMorrow, H. M. Ronnow, B. Lake, S. M. Hayden, G. Aeppli, T. G. Perring, M. Mangkorntong, M. Nohara, and H. Tagaki, Phys. Rev. Lett. **93**, 147002 (2004).
[30] M. Fujita, H. Goka, K. Yamada, and M. Matsuda, Phys. Rev. B **66**, 184503 (2002).
[31] B. Khaykovich, Y. S. Lee, R. W. Erwin, S. H. Lee, S. Wakimoto, K. J. Thomas, M. A. Kastner, and R. J. Birgeneau, Phys. Rev. B **66**, 014528 (2002).
[32] Y. S. Lee, R. J. Birgeneau, M. A. Kastner, Y. Endoh, S. Wakimoto, K. Yamada, R. W. Erwin, S. H. Lee, and G. Shirane, Phys. Rev. B **60**, 3643 (1999).
[33] S. Katano, M. Sato, K. Yamada, T. Suzuki, and T. Fukase, Phys. Rev. B **62**, R14677 (2000).
[34] H. Kimura, H. Matsushita, K. Hirota, Y. Endoh, K. Yamada, Y. S. Lee, M. A. Kastner, and R. J. Birgeneau, J. Phys. Chem. Solids **60**, 1067 (1999).
[35] O. Zachar, S. A. Kivelson, and V. J. Emery, Phys. Rev. B **57**, 1422 (1998).
[36] G. Shirane, S. M. Shapiro, and J. M. Tranquada, *Neutron Scattering with a Triple-Axis Spectrometer* (Cambridge University Press, Cambridge, 2002).
[37] G. L. Squires, *Introduction to the Theory of Thermal Neutron Scattering* (Dover, New York, 1996).
[38] J. M. Tranquada, in *Treatise of High Temperature Superconductivity*, edited by J. Robert Schrieffer, arXiv:cond-mat/0512115.
[39] S. Wakimoto, R. J. Birgeneau, Y. Fujimaki, N. Ichikawa, T. Kasuga, Y. J. Kim, K. M. Kojima, S.-H. Lee, H. Niko, J. M. Tranquada, S. Uchida, and M. v. Zimmermann, Phys. Rev. B **67**, 184419 (2003).
[40] P. Wochner, J. M. Tranquada, D. J. Buttrey, and V. Sachan, Phys. Rev. B **57**, 1066 (1998).
[41] J. M. Tranquada, N. Ichikawa, and S. Uchida, Phys. Rev. B **59**, 14712 (1999).
[42] P. Dai, H. A. Mook, R. D. Hunt, and F. Dogan, Phys. Rev. B **63**, 054525 (2001).
[43] M. Arai, T. Nishijima, Y. Endoh, T. Egami, S. Tajima, K. Tomimoto, Y. Shiohara, M. Takahashi, A. Garrett, and S. M. Bennington, Phys. Rev. Lett. **83**, 608 (1999).
[44] P. Bourges, Y. Sidis, H. F. Fong, L. P. Renault, J. Bossy, A. Ivanov, and B. Keimer, Science **288**, 1234 (2000).
[45] J. M. Tranquada, B. J. Sternlieb, J. D. Axe, Y. Nakamura, and S. Uchida, Nature (London) **375**, 561 (1995).
[46] J. M. Tranquada, D. J. Buttrey, J. E. Lorenzo, and V. Sachan, Physica B **213**, 69 (1995).
[47] V. Sachan, D. J. Buttrey, J. M. Tranquada, J. E. Lorenzo, and G. Shirane, Phys. Rev. B **51**, 12742 (1995).
[48] J. M. Tranquada, D. J. Buttrey, and V. Sachan, Phys. Rev. B **54**, 12318 (1996).
[49] J. M. Tranquada, H. Woo, T. G. Perring, H. Goka, G. Gu, G. Xu, M. Fujita, and K. Yamada, J. Phys. Chem. Solids **67**, 511 (2006).
[50] C. Stock, W. J. L. Buyers, R. A. Cowley, P. S. Clegg, R. Coldea, C. D. Frost, R. Liang, D. Peets, D. Bonn, W. N. Hardy, and R. J. Birgeneau, Phys. Rev. B **71**, 024522 (2005).
[51] S.-H. Lee, S.-W. Cheong, K. Yamada, and C. F. Majkrzak, Phys. Rev. B **63**, 060405(R) (2001).
[52] P. G. Freeman, A. T. Boothroyd, D. Prabhakaran, M. Enderle,

and C. Niedermayer, Phys. Rev. B **70**, 024413 (2004).
[53] S.-H. Lee, J. M. Tranquada, K. Yamada, D. J. Buttrey, Q. Li, and S.-W. Cheong, Phys. Rev. Lett. **88**, 126401 (2002).
[54] A. T. Boothroyd, P. G. Freeman, D. Prabhakaran, A. Hiess, M. Enderle, J. Kulda, and F. Altorfer, Phys. Rev. Lett. **91**, 257201 (2003).
[55] J. M. Tranquada, J. D. Axe, N. Ichikawa, Y. Nakamura, S. Uchida, and B. Nachumi, Phys. Rev. B **54**, 7489 (1996).
[56] V. J. Emery, S. A. Kivelson, and J. M. Tranquada, Proc. Natl. Acad. Sci. U.S.A. **96**, 8814 (1999).
[57] A. Boothroyd (private communication).